Earth and Planetary Science Letters 379 (2013) 38–48

Contents lists available at ScienceDirect

Earth and Planetary Science Letters

www.elsevier.com/locate/epsl

Experimental evidence for Mo isotope fractionation between metal and silicate liquids

Remco C. Hin [a,*,1], Christoph Burkhardt [a], Max W. Schmidt [a], Bernard Bourdon [a,b], Thorsten Kleine [c]

[a] Institute for Geochemistry and Petrology, ETH Zurich, Clausiusstrasse 25, 8092 Zurich, Switzerland
[b] Ecole Normale Supérieure de Lyon, CNRS and UCBL, 46 Allée d'Italie, 69364 Lyon Cedex 07, France
[c] Institut für Planetologie, Westfälische Wilhelms-Universität Münster, Wilhelm Klemm-Strasse 10, 48149 Münster, Germany

ARTICLE INFO

Article history:
Received 8 November 2012
Received in revised form 17 June 2013
Accepted 2 August 2013
Available online xxxx
Editor: B. Marty

Keywords:
Mo isotopes
metal–silicate experiments
stable isotope fractionation
core formation

ABSTRACT

Stable isotope fractionation of siderophile elements may inform on the conditions and chemical consequences of core–mantle differentiation in planetary objects. The extent to which Mo isotopes fractionate during such metal–silicate segregation, however, is so far unexplored. We have therefore investigated equilibrium fractionation of Mo isotopes between liquid metal and liquid silicate to evaluate the potential of Mo isotopes as a new tool to study core formation. We have performed experiments at 1400 and 1600 °C in a centrifuging piston cylinder. Tin was used to lower the melting temperature of the Fe-based metal alloys to <1400 °C, while variable Fe-oxide contents were used to vary oxygen fugacity in graphite and MgO capsules. Isotopic analyses were performed using a double spike technique. In experiments performed at 1400 °C, the $^{98}Mo/^{95}Mo$ ratio of silicate is 0.19 ± 0.03‰ (95% confidence interval) heavier than that of metal. This fractionation is not significantly affected by the presence or absence of carbon. Molybdenum isotope fractionation is furthermore independent of oxygen fugacity in the range IW −1.79 to IW +0.47, which are plausible values for core formation. Experiments at 1600 °C show that, at equilibrium, the $^{98}Mo/^{95}Mo$ ratio of silicate is 0.12 ± 0.02‰ heavier than that of metal and that the presence or absence of Sn does not affect this fractionation. Equilibrium Mo isotope fractionation between liquid metal and liquid silicate as a function of temperature can therefore be described as $\Delta^{98/95}Mo_{Metal-Silicate} = -4.70(\pm 0.59) \times 10^5/T^2$. Our experiments show that Mo isotope fractionation may be resolvable up to metal–silicate equilibration temperatures of about 2500 °C, rendering Mo isotopes a novel tool to investigate the conditions of core formation in objects ranging from planetesimals to Earth sized bodies.

1. Introduction

The segregation of a metallic core from a silicate mantle is arguably the largest differentiation event in growing planetary objects. Core formation in terrestrial planets may have involved merging of metal cores derived from already differentiated objects added during accretion (Karato and Murthy, 1997; Rubie et al., 2011; Taylor et al., 1993). Alternatively or complementary, it may have been associated with metal–silicate equilibration in a deep magma ocean (e.g. Li and Agee, 1996; Righter and Drake, 1996; Wood et al., 2006). In the former case, the chemical signatures of core formation would reflect those of the relatively low temperatures and pressures characteristic for the planetesimals and planetary embryos constituting the building blocks of the Earth. In the latter case, they would be the result of metal–silicate equilibration at the high pressures and temperatures prevailing in the deep Earth. Most of the information about the conditions of core formation has come from studies of elemental distributions combined with experimental studies of element partitioning between metal and silicate liquids (e.g. Li and Agee, 1996; Righter and Drake, 1996; Wood et al., 2006). As a result of these studies, equilibrium models of core formation in growing planets have become favoured over disequilibrium models, because the observed abundances of siderophile elements in the Earth's mantle match those predicted for metal–silicate equilibration at high temperatures and pressures in a deep magma ocean (Corgne et al., 2008; Righter et al., 2010; Wood et al., 2006). However, more recently it was shown that disequilibrium models provide an equally good match to the observed siderophile element abundances, indicat-

* Corresponding author.
E-mail address: remco.hin@bristol.ac.uk (R.C. Hin).
[1] Present address: School of Earth Sciences, University of Bristol, Queens Road, Bristol BS8 1RJ, United Kingdom.

0012-821X/$ – see front matter
http://dx.doi.org/10.1016/j.epsl.2013.08.003

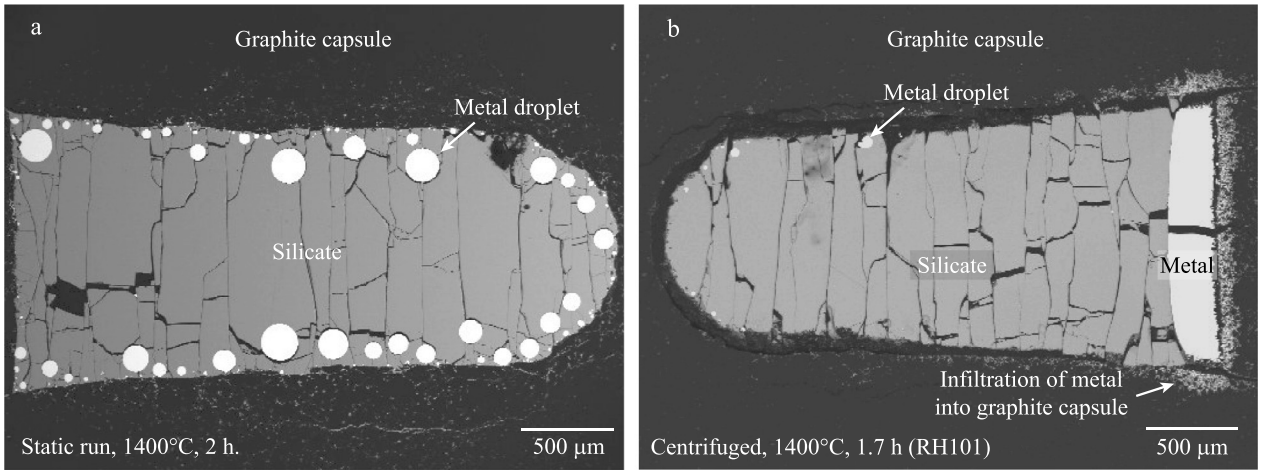

Fig. 1. Backscattered electron images of experiments performed in a standard piston cylinder (panel a) and a centrifuging piston cylinder (panel b). Although metal and silicate liquids can segregate well during standard piston cylinder runs, this is not always the case (panel a). Centrifugation ascertains good separation of the two liquids (panel b), except that surface tension often retains a few metal droplets attached to the capsule wall, particularly in graphite capsules.

ing that elemental partitioning studies alone cannot be used to constrain the degree of metal–silicate equilibration during core formation (Rudge et al., 2010). Furthermore, Rubie et al. (2011) concluded that a model with incomplete re-equilibration of the accreting material best reproduces the element budget of the silicate Earth.

Stable isotopes have emerged as a tool to constrain the conditions of core formation (e.g. Georg et al., 2007; Moynier et al., 2011; Zhu et al., 2002). Mass dependent equilibrium fractionation of isotopes occurs due to differences in the bond stiffness of isotopes between various phases and it is a strong function of temperature (Bigeleisen and Mayer, 1947; Urey, 1947). In principle, isotope fractionation factors could be calculated from vibrational frequencies of the isotopes in both phases (Bigeleisen and Mayer, 1947; Schauble, 2004; Urey, 1947), but these frequencies remain poorly constrained for most elements and phases. Thus, experimental calibration of the magnitude and direction of mass dependent isotope fractionation between metal and silicate is the best method to develop stable isotopes as tracers of core formation. For example, such experimental calibrations showed that Si isotopes fractionate between metal and silicate at conditions relevant for core formation (Shahar et al., 2011), as opposed to Fe and Ni isotopes (Hin et al., 2012; Lazar et al., 2012; Poitrasson et al., 2009).

Molybdenum is an element of interest for core formation. It is refractory in the canonical solar nebula (Fegley and Palme, 1985) and its siderophile behaviour suppresses the necessity for mass balance calculations, because bodies with core mass fractions as small as 5% will have over 90% of their Mo in the metallic core. As such, the isotopic effect is quantitatively transferred to the silicate portion, making analyses of silicate samples sufficient to study metal–silicate fractionation.

We present the first experimental study of Mo isotope fractionation between liquid metal and liquid silicate. To determine whether there is resolvable fractionation, we have performed experiments in a centrifuging piston cylinder, which separated the metal from the silicate prior to chemical processing for isotopic analyses. Controlled variables included temperature, oxygen fugacity, the metal composition, and some variation in silicate melt polymerisation. Although no data are yet available on natural rocks, our results indicate that Mo isotopes constitute a suitable tool to determine in particular temperatures of core formation in planetary bodies.

2. Methods

2.1. Experimental methods

Molybdenum is classified as a moderately siderophile element, but its metal/silicate liquid partitioning may exceed 1000 at oxygen fugacities relevant for core formation (Holzheid et al., 1994; Wade et al., 2012). Such elemental distribution implies that a silicate melt contaminated by ~0.03 vol% metal consists of an approximately 1:1 mixture by mass of metallic Mo and Mo-oxide. Segregation of the metal and silicate liquids prior to isotopic analysis is therefore essential for a reliable interpretation of the isotopic data. In standard piston cylinder experiments, the metal remains sometimes dispersed and we therefore used a centrifuging piston cylinder at ETH Zurich to ascertain good density segregation of the two synthetic liquids (Fig. 1). Such centrifugation does not cause compositional gradients that could induce isotopic fractionation, as can be deduced from the results of centrifuged and static experiments in Hin et al. (2012).

Equilibrium isotope fractionation decreases strongly as a function of temperature, favouring low temperatures to analytically resolve fractionation. We have thus performed experiments at 1400 °C and 1600 °C, at pressures of 1 GPa. The melting temperature of Fe–Mo alloys (>1500 °C) was lowered with Sn to <1400 °C (Okamoto, 1993). Both Sn-bearing and Sn-free experiments were performed at 1600 °C to control for potential effects of Sn on the Mo isotope fractionation factors (Table 1, cf. mixtures B and F). Silicates were prepared from purified oxides, except for Ca, Na and K that were purchased as carbonates and mixed with SiO_2 (and Al_2O_3) to synthesise wollastonite, albite and orthoclase after decarbonation. The silicate and metal fractions were finely mixed into a bulk powder. Graphite as well as MgO capsules were employed to establish whether carbon affects Mo isotope fractionation, because element partitioning may be affected by carbon (Jana and Walker, 1997).

Run durations were varied to assess isotopic equilibration, while oxygen fugacity was varied to potentially assess the effect of Mo^{4+}/Mo^{6+} in the silicate melt on isotopic fractionation. We varied oxygen fugacity by varying the concentration of Fe_2O_3 in the oxide component of the starting material from 6.42 to 44.7 wt% (recalculated to FeO in Table 1; mixtures B, C, D). These runs were all performed at 1400 °C.

A consequence of the siderophile character of Mo is that high Mo concentrations in the metal are required to yield measurable

Table 1
Compositions (wt%) of starting mixtures. Weight fractions (f) of metal and silicate (subscripts M and Sil, respectively) are given at the bottom.

	A	B1	B2	C	D	E	F
Metal							
Fe	66.9	72.0	72.0	71.3	71.2	77.0	92.3
Sn	27.2	20.1	20.3	19.1	20.7	21.7	
Mo	5.83	7.82	7.76	9.59	8.09	1.25	7.65
Silicate							
SiO_2	47.9	49.0	55.2	52.8	47.9	49.5	54.2
Al_2O_3	4.51	2.92	2.10	8.61	1.47	1.87	2.26
MgO	4.43	3.51	1.37	8.49	0.99	6.93	1.45
FeO[1]	27.1	29.2	28.1	5.78	40.2	28.7	29.0
CaO	12.0	11.0	9.06	18.5	4.08	8.88	8.90
Na_2O	1.02	1.03	0.68	4.16	0.89	0.68	0.67
K_2O	0.00	0.00	0.29	1.02	0.00	0.30	0.28
O[1]	3.0	3.3	3.1	0.6	4.5	3.2	3.2
f_M	0.3449	0.3556	0.3494	0.3321	0.3475	0.3501	0.3445
f_{Sil}	0.6551	0.6444	0.6506	0.6679	0.6525	0.6499	0.6555

[1] Iron-oxide was added to the starting mixture as Fe_2O_3, but has been recalculated (based on molar masses) to FeO here for better comparison to EPMA data of the experimental run products. Consequently, the oxides in this table do not sum to 100% and the difference to 100% is shown as excess oxygen.

quantities of Mo in the silicate. We have therefore doped the metal component of our starting mixtures with 5–10 wt% Mo and prepared bulk starting mixtures with approximately 65 wt% silicate component. Under natural conditions, however, Mo concentrations in metals are generally below 50 ppm. We have therefore performed one experiment with a starting mixture with 1.25 wt% Mo in the metal component to verify that, as to be expected, the high concentrations of Mo in our experiments do not affect isotopic fractionation (Table 1, mixture E).

All different starting mixtures were prepared using the same metallic Mo powder and all experiments were performed with talc/pyrex assemblies in a 14 mm bore centrifuging piston cylinder. B-type thermocouples were protected by mullite (1400 °C) or Al_2O_3 (1600 °C) sleeves, while crushable MgO was used as spacers. The graphite and MgO capsules were welded into $Au_{50}Pd_{50}$ or Pt jackets with an outer diameter of 4.0 mm. Based on temperature calibrations in these assemblies (Hin et al., 2012), the volume of metal liquid should have had an average temperature that was maximum 3.5 °C lower than the average temperature of the silicate melt. Further technical specifications and details of experimental protocols for the centrifuging piston cylinder at ETH Zurich are provided in Schmidt et al. (2006) and Hin et al. (2012).

2.2. Analytical methods

2.2.1. Elemental compositions

Elemental concentrations were analysed on polished and carbon-coated samples with a Jeol JXA 8200 electron microprobe equipped with 5 spectrometers. An acceleration voltage of 15 kV was employed for all analyses. Silicates were analysed with a 6 nA current and a beam diameter of 1–10 µm, while metals were analysed with a 20 nA current and a beam diameter of 10 µm. Standards consisted of pure metals for metal compositions, and natural and synthetic silicates and oxides for silicate compositions, except for SnO_2 that was analysed relative to a metallic Sn standard. Approximately ten spots were analysed on each phase.

Molybdenum contents in the silicate melt were always below microprobe detection limits. Molybdenum concentrations were therefore determined by isotope dilution (see below) and for selected samples by laser ablation ICPMS (see electronic Supplementary Material).

2.2.2. Isotopic compositions

After determination of elemental compositions, metal and silicate in each sample were separated and removed from the capsule with a diamond wire saw (300 µm wire diameter). A previously unused diamond wire was employed to prevent contamination. Furthermore, each analysed phase was carefully cleaned with 30 µm alumina grinding paper to remove contamination from sawing. This also removed tiny metal droplets that had stuck to the capsule walls during centrifugation. The clean bulk pieces of silicate or metal were sonicated in acetone for 5 min. They were then crushed under acetone with separate Al_2O_3 pestles and mortars for metal and silicate that had previously not been used to crush Mo-bearing materials. A final inspection with a binocular microscope ensured that no visible metal contamination occurred in the silicate.

All samples were weighed in pre-cleaned 15 ml Savillex beakers and were digested in 2:1 mixtures of 14 M HNO_3 and 24 M HF (silicate samples and starting materials) or in 6 M HCl with a few drops of 14 M HNO_3 (metals). A ^{100}Mo–^{97}Mo double spike (see electronic Supplementary Material for calibration details) was added to silicate samples prior to digestion, while starting materials and metal samples were digested before the double spike was added to an aliquot of the dissolved starting material or metal. The spiked aliquots were equilibrated overnight on a hotplate (130 °C). After digestion and spike-sample equilibration, all samples were dried down and treated with 1:1 mixtures of 14 M HNO_3 and 30% H_2O_2 to remove any remaining organic material.

A four-stage ion exchange procedure subsequently separated Mo from its matrix. Three of the four stages are identical to the protocol of Burkhardt et al. (2011), except that resin volumes for the first and second stages were scaled down from 14 and 7 ml to 3 and 2 ml, respectively, as our samples never exceeded masses of 20 mg. The first of these three stages employed a cation resin (Dowex AG50W-X8), onto which the samples were loaded in 1 ml 1 M HCl–0.1 M HF. The loaded solution was collected together with an additional 4 ml 1 M HCl–0.1 M HF. This stage separates Mo from a large portion of its matrix. The second stage employed anion resin (Biorad AG1-X8). Samples were loaded in 6 ml 1 M HF, followed by rinsing with 12 ml 1 M HF, 16 ml 6 M HCl–1 M HF and 2 ml ultra-pure H_2O to remove remaining matrix (particularly Fe and Zr contaminants). Molybdenum was then eluted with 6.5 ml 3 M HNO_3. A TRU-spec resin was finally used to ensure that any remaining fractions of Zr and Ru were removed. Samples were loaded on the 1 ml TRU Spec resin in 1 ml 1 M HCl and rinsed with additional 6 ml 1 M HCl before Mo was eluted with 6.5 ml 0.1 M HCl.

An additional ion exchange step was placed between the original first and second stages to remove Sn. This was done by eluting Mo from an anion resin (2 ml AG1-X8) with 1 M HCl, making use of the different distribution coefficients of Mo and Sn under these conditions (Mizuike, 1983). The resin was equilibrated twice with 4 ml 1 M HCl prior to loading of the samples in 1 ml 1 M HCl. This 1 ml of sample was not collected after elution, but the following 13 ml 1 M HCl were collected and then dried to prepare for the next stages described above. Molybdenum blanks for the full procedure generally varied between 100 and 250 pg and their $\delta^{98/95}$Mo (see below for definition) varied between +1 and −1‰. Even in the most extreme case, this resulted in <0.008‰ blank contribution on $\delta^{98/95}$Mo and blank corrections were therefore not necessary.

The isotopic analyses were performed on two different multi-collector inductively coupled plasma mass spectrometers (MC-ICPMS). At ETH Zurich, a Nu Instruments Plasma 1700 equipped with a DSN-100 desolvator and PFA nebuliser was employed. On-peak baselines were collected for 60 s prior to each analysis. All seven isotopes of Mo were collected in 40 scans of 5 s integration together with ^{90}Zr and ^{99}Ru to monitor interferences. Zr/Mo and Ru/Mo were $<5 \times 10^{-5}$ during most analyses, which resulted in corrections of <0.01‰ on $\delta^{98/95}$Mo values. Double spike-sample

mixtures were typically analysed as solutions of 75–100 ppb total Mo, yielding total Mo intensities of approximately 14×10^{-11} A at an uptake rate of ~140 µl min^{-1}. This protocol consumed about 45–60 ng total Mo (corresponding to 23–30 ng sample Mo) per analysis.

Experiments run at an oxygen fugacity more than one log unit below the iron–wüstite buffer yielded too low amounts of Mo in the silicate melt for multiple analyses on the Nu1700 at ETH Zurich. They were therefore analysed on a ThermoScientific Neptune Plus at the Westfälische Wilhelms-Universität Münster. Measurement protocols were identical to those described for the Nu1700, except that ^{91}Zr instead of ^{90}Zr was measured to monitor Zr interferences and that on-peak backgrounds were collected for 30 s prior to each analysis. Furthermore, normal H cones were used and samples were introduced with a Cetac Aridus II desolvator after aspiration with a PFA nebuliser. Solutions of 50 ppb total Mo were analysed (consuming ~24 ng total Mo per analysis), which yielded a total Mo intensity of about 14×10^{-11} A at an uptake rate of ~100 µl min^{-1}.

Data reduction was performed for all analyses with the geometrically motivated double spike deconvolution scheme of Siebert et al. (2001), using the evaluation software of Nu Instruments Ltd. The reduction employed NIST SRM 3134 as reference standard. The molar proportion of spike determined with this reduction scheme was used to calculate Mo concentrations of all silicate samples. Moreover, the natural fractionation factor of a sample (α_{Sample}) obtained from the deconvolution was used to calculate the reported $\delta^{98/95}$Mo relative to NIST SRM 3134. As previously observed in double spiked isotope analyses, average compositions of the reference standard within a measurement session often deviate slightly from zero (Schoenberg et al., 2008; Siebert et al., 2001). A correction was made for this by subtracting the average composition of NIST SRM 3134 in a measurement session ($\alpha^{Mean}_{SRM3134}$) from each sample analysis in the same session, such that:

$$\delta^{98/95}\mathrm{Mo} = 1000\left(\alpha_{Sample} - \alpha^{Mean}_{SRM3134}\right)\ln\left(\frac{m_{98}}{m_{95}}\right) \quad (1)$$

where m_{98} and m_{95} are the atomic masses of ^{98}Mo and ^{95}Mo, respectively. Analytical uncertainties on sample compositions are reported as the 95% confidence interval (95% c.i.) (see Table 3).

Long-term reproducibility (2SD) over the course of this study was evaluated on the NIST SRM 3134 standard as well as on aliquots of BHVO-2 powder and a solution of molybdenite sample AJ011 (Greber et al., 2011). Spiked runs of NIST SRM 3134 standard yielded an average $\delta^{98/95}$Mo of 0.00 ± 0.09‰ (2SD) on the Nu1700 ($n = 159$) and 0.00 ± 0.05‰ on the Neptune Plus ($n = 131$). Averages for BHVO-2 on the Nu1700 and Neptune Plus are -0.07 ± 0.13‰ ($n = 16$ on 5 aliquots) and -0.06 ± 0.05‰ ($n = 15$ on 2 aliquots), while those for AJ011 are 0.70 ± 0.12‰ ($n = 6$ on 2 aliquots) and 0.70 ± 0.06‰ ($n = 12$ on 2 aliquots). These latter values are within analytical uncertainty identical to those of Greber et al. (2011), when corrected to the same reference standard. In addition, we analysed an aliquot of the JMC Mo standard from the University of Bern, which gave an average of -0.26 ± 0.03‰ (2SD), which compares well to the value of -0.25 ± 0.09‰ (2SD) as determined by Greber et al. (2012).

Fractionation factors (Δ) between metal and silicate are presented as differences between the bulk isotopic composition of the starting mixture and the analysed silicate composition. This is done because elemental Mo concentrations in the metal exceed those in the silicate by a factor ~1500, i.e. >99.9% of the bulk Mo resides in the metal phase. Thus, a fractionation of >9‰ between metal and silicate would be required to shift the metal by 0.05‰ relative to the bulk composition, while a fractionation of 0.2‰ would shift the metal <0.002‰ relative to the bulk. Metal isotopic compositions are thus not analytically resolvable from isotopic compositions of bulk starting mixtures, such that

$$\Delta^{98/95}\mathrm{Mo}_{Metal-Silicate} = \Delta^{98/95}\mathrm{Mo}_{Bulk-Silicate} = \delta^{98/95}Mo_{Bulk} - \delta^{98/95}\mathrm{Mo}_{Silicate} \quad (2)$$

3. Results

Major element compositions of the melts are presented in Table 2 and Table S2. Elemental Mo contents in silicates together with isotopic compositions as well as all details of experimental run conditions are presented in Table 3.

3.1. Textures and elemental compositions

In general, experiments were performed at temperatures exceeding the liquidi of metal alloys as well as of the silicate mixtures in both graphite (Fig. 1b) and MgO (Fig. 2a) capsules. The liquidus of the silicate melt was not reached only in experiments performed at 1600 °C in MgO capsules, where rapid dissolution of MgO from the capsule led to a significant shift in melt composition and to olivine saturation (Fig. 2b and Fig. S3a). For the same reason, the MgO capsule contact was covered by a film of <25 µm sized olivine crystals in experiments at 1400 °C (Fig. S3b, c). Centrifugation has separated the metal liquids from the silicate liquids, except for a few small metal droplets that stuck to the capsule walls, in particular in graphite capsules (Fig. 1b). These droplets were removed by grinding the exterior portions of the silicate glass cylinders (see Section 2.2.2). Detailed inspection by SEM indicated that no tiny (0.1–10 µm) metal droplets were present in the quenched silicate melt (Fig. 2c–f and Fig. S3b–d).

Molybdenum contents in metal alloys have increased by 5–45% relative to the starting mixtures, while Sn (only added in metal form) was oxidised to form 0.21 to 4.36 wt% SnO_2 in the silicate melt. In one experiment (RH76) a separate ~$Pd_{40}Sn_{60}$ alloy formed in addition to a relatively Sn-poor Fe–Mo alloy (Table S2). Mo was below microprobe detection limits (~0.03 wt%) in the Pd–Sn alloy, and hence the formation of the Pd–Sn alloy could not have modified the Mo isotope composition of the Fe–Mo–Sn alloy. The formation of such a Pd–Sn alloy in a single experiment is readily explained by diffusive exchange of the Fe–Sn–Mo alloy with the Au–Pd capsule.

Except for SnO_2, most oxides in the silicate melt from experiments in MgO capsules have been diluted by MgO dissolution from the capsule. Only FeO contents in experiments performed in MgO capsules with starting mixture C have increased from 5.78 wt% to about 8.4 wt%, despite the increase in MgO contents from 8.49 wt% to about 15 wt%. MgO dissolution at 1600 °C has been much more extensive than at 1400 °C: after 1.1 h MgO contents in the silicate melt in experiment RH80 had increased from 1.37 wt% to 24.4 wt%, which compares to an increase to 16.0 wt% after 4.0 h at 1400 °C in experiment RH77. No major element compositional gradients were observed in any of the melts.

Oxygen fugacity was calculated relative to the iron–wüstite buffer (ΔIW) with the following equation:

$$\Delta\mathrm{IW} = 2 \cdot \log\left(\frac{X_{FeO} \cdot \gamma_{FeO}}{X_{Fe} \cdot \gamma_{Fe}}\right) \quad (3)$$

where X_{FeO} and X_{Fe} are the molar fractions of FeO and Fe in the silicate and metal melts, respectively, while γ_{FeO} and γ_{Fe} are their respective activity coefficients. Activity coefficients for metallic Fe were calculated with the modified Wagner epsilon approach of Ma (2001). The interaction parameter ε^{Sn}_{Mo} was determined to be −4.94 at 1873 K based on the Sn-free and Sn-bearing experiments RH102 and RH103, again following the approach of Ma (2001).

Table 2
Elemental compositions (wt%) of selected samples with their experimental run conditions. P = pressure (GPa), T = temperature (°C), fO_2 = oxygen fugacity relative to the iron–wüstite buffer (ΔIW), t = run duration in hour.

	Start mix B1		Start mix B2		Start mix C		Start mix D		Start mix E		Start mix F		Start mix F	
	RH72	2SD	RH82	2SD	RH97	2SD	RH101	2SD	RH99	2SD	RH102	2SD	RH86[3]	2SD
P (GPa)[1]	0.91	0.08	0.91	0.06	0.98	0.04	0.95	0.04	0.89	0.05	0.10	0.09	0.95	0.02
T (°C)	1400		1400		1400		1400		1400		1600		1600	
t (h)	1.5		2.2		1.5		1.7		1.5		1.2		0.8	
fO_2 (ΔIW)	0.14		−0.64		−1.68		0.47		−0.52		0.06		−0.73	
Capsule type	Graphite		MgO		MgO		Graphite		MgO		Graphite		MgO	
Metal jacket	$Au_{50}Pd_{50}$		Pt		Pt		Pt		Pt		Pt		Pt	
Metal														
Fe	73.2	1.7	67.8	4.8	68.9	1.5	73.8	0.5	72.4	5.1	85.4	0.8	89.2	4.6
Sn	12.5	1.1	22.8	4.2	21.1	0.4	9.04	0.43	26.2	5.3	n.a.	n.a.	n.a.	n.a.
Mo	9.86	1.00	9.81	1.83	10.2	1.5	11.8	0.5	1.66	0.13	9.21	0.76	9.79	4.22
Pt	n.a.	n.a.	0.09	0.12	0.06	0.04	0.01	0.03	0.04	0.05	0.04	0.05	0.10	0.09
Pd	0.14	0.13	n.a.	n.a.	n.a.	n.a.	n.a.	n.a.	n.a.	n.a.	n.a.	n.a.	n.a.	n.a.
Total	95.7	0.4	100.6	1.2	100.5	0.7	94.9	0.4	100.3	0.4	94.8	1.1	99.3	0.6
C (calc)[2]	4.3						5.1				5.2			
Silicate														
SiO_2	42.8	1.1	46.0	5.7	45.8	0.9	39.9	0.8	42.4	5.6	46.9	0.6	38.5	0.9
Al_2O_3	2.47	0.13	1.67	0.68	7.25	0.21	1.22	0.12	1.65	0.94	1.97	0.12	2.45	1.19
MgO	3.10	0.18	14.3	8.9	14.4	0.4	0.85	0.10	12.5	11.3	1.32	0.09	18.3	4.0
FeO	37.1	0.6	28.6	5.6	8.71	0.39	49.0	1.6	32.5	4.8	40.4	0.6	30.4	5.1
CaO	9.55	0.26	7.27	4.88	16.7	0.7	3.39	0.42	7.91	6.92	8.05	0.19	9.62	0.74
Na_2O	0.97	0.13	0.56	0.34	3.66	0.26	0.83	0.12	0.66	0.43	0.64	0.10	0.86	0.24
K_2O	0.00	0.01	0.24	0.12	0.92	0.15	0.01	0.02	0.27	0.11	0.23	0.03	0.33	0.17
SnO_2	3.03	0.95	1.14	0.84	0.26	0.10	4.06	0.39	0.94	0.77	0.00	0.00	0.01	0.02
Total	99.0	1.1	99.7	1.6	97.8	0.8	99.2	1.3	98.8	1.7	99.5	0.9	100.4	0.7

[1] Errors refer to the time dependent variation of the pressure in centrifuge experiments. They are calculated as the 2SD of the pressure registrations in 30 s intervals in our log files.
[2] Carbon contents are calculated as the difference of the totals from 100%.
[3] Owing to the larger olivine quench crystals occurring in experiments in MgO capsules at 1600 °C, the silicate composition of this sample is derived from a mass balance calculation based on the analysed compositions of the olivine quench crystals and the glassy matrix.

All other interaction parameters were taken from the Steelmaking Data Sourcebook (1988). Holzheid et al. (1997) determined that the activity coefficient of FeO in silicate liquid is constant at 1.7 between 1300 and 1600 °C for broadly basaltic compositions with up to 20 wt% MgO and 12 wt% FeO. They also determined an FeO activity coefficient of 1.7 in an experiment with 26.0 wt% FeO and 4.87 wt% MgO, but some of our experiments have up to 49.0 wt % FeO, falling outside the range of Holzheid et al. (1997). In the absence of better approximations, we have kept γ_{FeO} constant at 1.7 in Eq. (3). Calculated ΔIW thus varied from −1.05 with starting mixture C to +0.47 with starting mixture D in graphite capsules, and from −1.79 with starting mixture C to −0.62 with starting mixture B2 in MgO capsules (Tables 3 and S2). We note, however, that Richardson (1956) found that FeO activities in CaO–FeO–SiO_2 melts approach Raoult's law behaviour at 50 mol% FeO. If an activity coefficient of 1.0 instead of 1.7 is selected, our most oxidised experiments yield a calculated oxygen fugacity (ΔIW) of 0.00 instead of +0.47.

Molybdenum contents in the silicate melts vary from 6.09 to 13.3 ppm at ΔIW below −1.0, and reach up to 119 ppm at ΔIW +0.47. High and variable Mo contents were observed for experiments in MgO capsules at 1600 °C (ΔIW about −0.7). They varied from 108 to 193 ppm after run durations of ∼0.75 h, and from 246 to 496 ppm after run durations of 1.1 h (Table 3).

3.2. Isotopic compositions

3.2.1. Starting material and metal melts

A total of three aliquots from starting mixtures B1 and F were analysed and yielded an average $\delta^{98/95}$Mo starting composition of -0.39 ± 0.02‰ (95% confidence interval). Equilibrated metal fractions from experiments RH55, RH76 and RH77 have $\delta^{98/95}$Mo compositions of -0.37 ± 0.04‰, -0.36 ± 0.06‰, and -0.38 ± 0.02‰ (95% c.i.), respectively, indistinguishable from the starting composition (Fig. 3 and Table 3).

3.2.2. Silicate melt from experiments at 1400 °C

Six experiments were performed with starting mixtures B1 and B2 at variable run durations from 0.5 to 7.0 h. Experiment RH71 with a run duration of 0.5 h resulted in a silicate $\delta^{98/95}$Mo of -0.28 ± 0.04‰ (95% c.i.). Silicates from the other five experiments are all within analytical uncertainty of each other, but generally slightly heavier than RH71, with $\delta^{98/95}$Mo between -0.18 ± 0.04‰ and -0.24 ± 0.10‰ (Fig. 4a and Table 3). The two experiments performed in MgO capsules (RH77 and RH82) have Mo isotope compositions indistinguishable from those performed in graphite capsules (Fig. 4a and Table 3).

In experiments with variable oxygen fugacity between ΔIW −1.79 and +0.47, the $\delta^{98/95}$Mo of the silicate melts varies between -0.14 ± 0.03‰ and -0.29 ± 0.02‰ (95% c.i.), but they do not correlate with oxygen fugacity (Fig. 4b). Again, no resolvable differences in $\delta^{98/95}$Mo occurred in experiments performed in graphite or MgO capsules (Fig. 4b and Table 3). The experiment performed with the lowest Mo content (1.66 wt% in the metal; experiment RH99) resulted in a silicate $\delta^{98/95}$Mo of -0.10 ± 0.02‰.

3.2.3. Silicate melt from experiments at 1600 °C

Sn-bearing as well as Sn-free experiments were performed at 1600 °C in both graphite and MgO capsules. Among both types of capsules, the Mo isotope composition of silicate melts from Sn-bearing and Sn-free experiments are within analytical uncertainty identical. However, there is a systematic offset between the $\delta^{98/95}$Mo compositions of silicates derived from graphite capsules and those derived from MgO capsules: the former vary from -0.26 ± 0.01‰ to -0.28 ± 0.01‰, while the latter vary from -0.33 ± 0.10‰ to -0.39 ± 0.07‰ (95% c.i.; Fig. 4a and Table 3).

4. Discussion

Analyses performed on metals from three experiments show that their $\delta^{98/95}$Mo compositions are within uncertainty identical

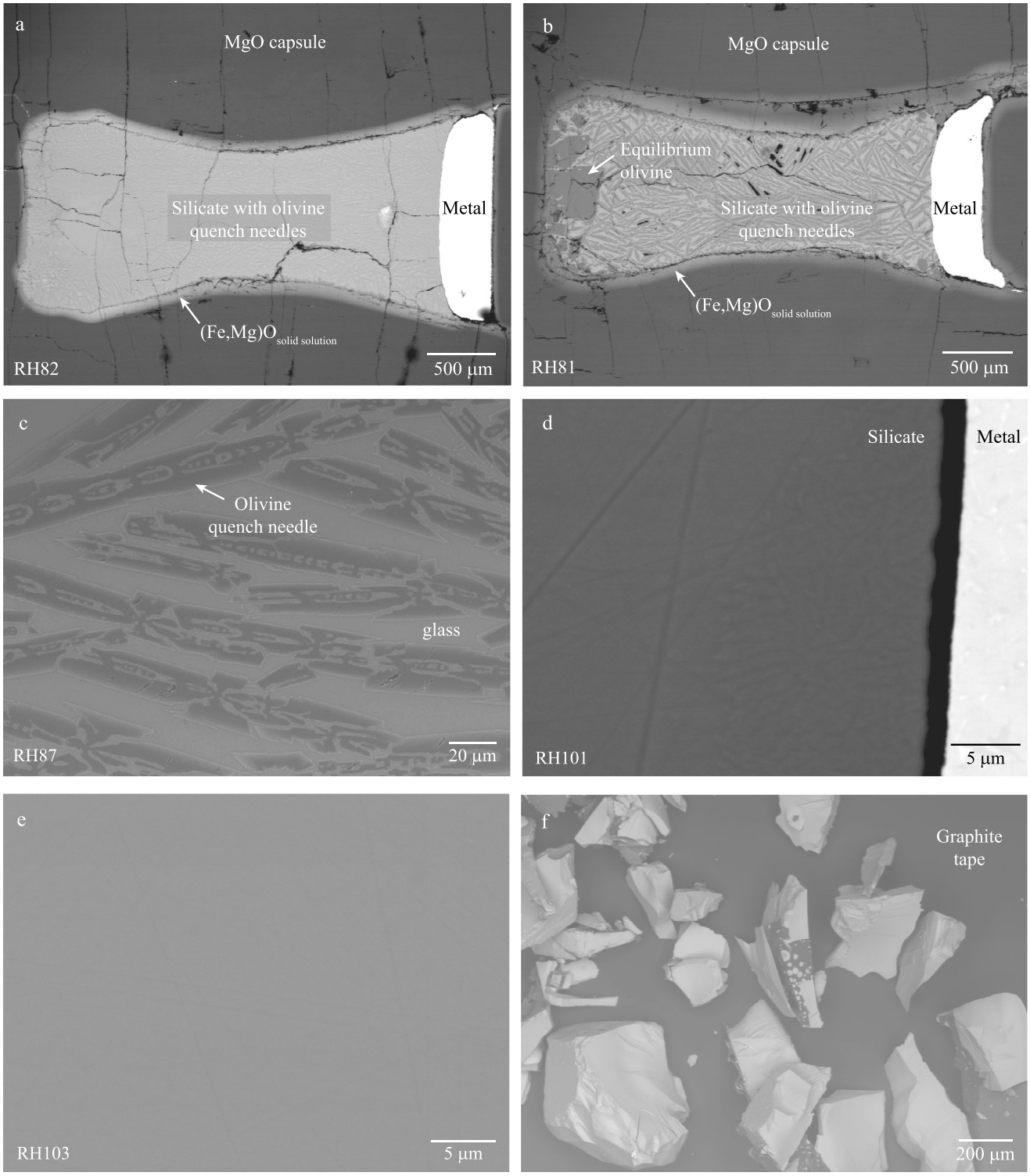

Fig. 2. Backscattered electron images of selected experiments. Panel (a) presents an example of an experiment performed in an MgO capsule at 1400 °C, which lacked significant euhedral olivine crystals and in which quench needles were barely visible. Panel (b) shows an experiment in an MgO capsule at 1600 °C with euhedral olivine crystals (a few hundred μm in size). Quench needles (olivine) in the silicate of the experiment are abundant (panel b, c). Panels (c–f) show details of polished (c–e) and crushed material (f) of the silicate products, to highlight that no indication of any metal presence has been observed.

Table 3
Isotopic compositions (relative to NIST SRM 3134) and details of experimental run conditions. Zurich = measurements performed on the Nu1700 at ETH Zurich; Münster = measurements performed on the Neptune Plus at Westfälische Wilhelms-Universität in Münster. P = pressure (GPa), T = temperature (°C), fO_2 = oxygen fugacity relative to the iron–wüstite buffer (ΔIW), t = run duration in hour, RCF = relative centrifugal force in multiples of the gravity constant (g), capsule type C = graphite.

Sample	Start mix	P (GPa)[1]	T (°C)	fO_2 (ΔIW)	t (h)	RCF (g)	Capsule type	$\delta^{98/95}$Mo (‰)	95% c.i. (‰)[2]	$\Delta^{98/95}Mo_{M\text{-}Sil}$ (‰)	95% c.i. (‰)	n[3]	[Mo] (ppm)[4]
Standards													
BHVO-2 (Zurich)								−0.07	0.13			16	
BHVO-2 (Münster)								−0.06	0.05			15	
AJ011 (Zurich)								0.70	0.12			6	
AJ011 (Münster)								0.70	0.06			12	
JMC Bern[5]								−0.26	0.02			6	
Starting mixture								−0.39	0.02			35	
Metals													
RH55 M	A		1350	0.10	4.0	487	C	−0.37	0.04			8	
RH76 M	B1		1400	0.13	7.0	393	C	−0.36	0.06			6	
RH77 M	B2		1400	−0.70	4.0	515	MgO	−0.38	0.02			6	
Silicates													
1400 °C													
RH55 Sil	A	0.79 ± 0.10	1350	0.10	4.0	487	C	−0.21	0.04	−0.18	0.04	4	52.5
RH71 Sil	B1	1.06 ± 0.10	1400	0.16	0.5	1130	C	−0.28	0.04	−0.11	0.05	9	73.3
RH72 Sil	B1	0.91 ± 0.08	1400	0.14	1.5	1140	C	−0.21	0.02	−0.18	0.03	8	74.9
RH74 Sil	B1	0.73 ± 0.17	1400	0.14	4.0	514	C	−0.20	0.04	−0.18	0.04	6	79.1
RH76 Sil	B1	0.82 ± 0.07	1400	0.13	7.0	393	C	−0.24	0.10	−0.15	0.10	4	71.2
RH94 Sil	C	0.97 ± 0.03	1400	−1.05	1.7	742	C	−0.14	0.03	−0.25	0.04	5	9.61
RH101 Sil	D	0.95 ± 0.04	1400	0.47	1.7	748	C	−0.22	0.02	−0.17	0.03	6	119
RH77 Sil	B2	0.90 ± 0.05	1400	−0.70	4.0	515	MgO	−0.18	0.04	−0.21	0.05	7	58.2
RH82 Sil	B2	0.91 ± 0.06	1400	−0.64	2.2	764	MgO	−0.19	0.04	−0.19	0.05	7	47.6
RH97 Sil	C	0.98 ± 0.04	1400	−1.68	1.5	764	MgO	−0.19	0.04	−0.20	0.05	5	6.09
RH98 Sil	C	1.00 ± 0.07	1400	−1.71	1.5	739	MgO	−0.29	0.02	−0.09	0.03	6	7.61
RH104 Sil	C	0.91 ± 0.04	1400	−1.79	4.0	489	MgO	−0.17	0.03	−0.22	0.04	6	13.3
RH99 Sil	E	0.89 ± 0.05	1400	−0.52	1.5	739	MgO	−0.10	0.02	−0.29	0.03	6	11.0
1600 °C													
RH92 Sil	B2	0.98 ± 0.08	1600	0.12	1.7	1070	C	−0.26	0.01	−0.13	0.02	6	52.6
RH103 Sil	B2	0.95 ± 0.17	1600	0.06	1.4	849	C	−0.28	0.01	−0.11	0.02	6	50.3
RH102 Sil	F	0.95 ± 0.09	1600	0.06	1.2	908	C	−0.27	0.02	−0.12	0.03	6	43.7
RH80 Sil	B2	1.00 ± 0.04	1600	−0.70	1.1	893	MgO	−0.35	0.06	−0.03	0.06	6	496
RH87 Sil	B2	1.06 ± 0.02	1600	−0.62	0.7	1863	MgO	−0.33	0.10	−0.06	0.10	3	193
RH81 Sil	F	0.98 ± 0.04	1600	−0.72	1.1	860	MgO	−0.37	0.11	−0.02	0.11	6	246
RH86 Sil	F	0.95 ± 0.02	1600	−0.73	0.8	1871	MgO	−0.39	0.07	0.00	0.07	6	108

[1] Errors are 2SD of the pressure variation during the experimental run, based on automatic log files with recordings every 30 s.
[2] 95% c.i. $= t_{0.95} \cdot SD/\sqrt{n}$ in which $t_{0.95}$ refers to a two-tailed 95% confidence Student-t test and SD is the standard deviation of the n repeated analyses.
[3] Number of isotopic analyses per sample or standard. Analyses were performed on single aliquots that were passed through chemistry once, except for standards (see text) and the starting mixture (two aliquots, of which one was passed through chemistry twice). Samples were analysed in two or three measurement sessions, apart from the starting mixture (nine sessions) and RH80, RH81 and RH87 (one session).
[4] Concentrations determined from double spiked isotope ratio analyses. Relative uncertainties (2SD) are better than 2% and are mainly dependent on weighing uncertainties of the small silicate sample masses (between 6 and 18 mg).
[5] JMC Bern = Johnson Matthey ICP standard (lot 602332B).

to the average bulk Mo isotope composition of the starting mixtures. This indicates closed system conditions for Mo in our experiments and confirms that the isotopic difference between the bulk starting mixtures and individual silicate melts recovered from the experiments can be equated to the difference in isotopic compositions between the equilibrated metal and silicate phases (Eq. (2)). As explained in Section 2.2.2, Mo isotope fractionation factors between metal and silicate liquids are thus obtained by subtracting silicate compositions from the composition of the bulk starting mixture.

4.1. Fractionation at 1400 °C

4.1.1. Time series

The results of the experimental time series imply that a run duration of 0.5 h is not sufficient to reach isotopic equilibrium at 1400 °C. The metal–silicate fractionation factor of RH71 is smaller by 0.08 ± 0.05‰ (95% c.i.) than the average of the other five experiments with run durations of 1.5 to 7.0 h. Based on diffusion coefficients of approximately 1.5×10^{-11} m^2 s^{-1} for Ti and Zr in haplobasaltic melt at 1400 °C (LaTourrette et al., 1996), we estimate that the diffusion length scale of Mo is <170 μm in the silicate melt in experiment RH71. Given the maximum length of the silicate melt of ~3 mm, it is conceivable that Mo isotopes had not fully equilibrated in this experiment. This resulted in kinetic enrichment of the silicate melt in light Mo isotopes by oxidation of metallic Mo and we have consequently excluded experiment RH71 from calculations of averages. Experiments run with a duration ⩾1.5 h, however, do not vary in Mo isotope fractionation factors, implying that open system behaviour with respect to Pd in some samples (RH74 and RH76) has not led to diffusion induced Mo isotope fractionation. We therefore conclude that these experiments display equilibrium fractionation of Mo isotopes, the silicate being on average 0.18 ± 0.03‰ (95% c.i.) lighter than metal.

Furthermore, experiments performed in graphite and MgO capsules yielded identical results at 1400 °C, implying that the presence of carbon has no resolvable effect on Mo isotope fraction-

ation. A similar observation was previously made by Hin et al. (2012) for Fe isotopes.

4.1.2. Fractionation as a function of oxygen fugacity

In silicate melts, Mo begins to increase valence state from 4+ to 6+ at an oxygen fugacity around ΔIW −1 (Farges et al., 2006; Holzheid et al., 1994; O'Neill and Eggins, 2002). Structural analyses by XANES imply that the change in valence state is accompanied by a structural modification from octahedral Mo^{4+} to tetrahedral Mo^{6+} coordination (Farges et al., 2006). As detailed in Schauble (2004), equilibrium mass dependent isotope fractionation is not only a function of mass and temperature, but also of bonding environment, the heavy isotopes concentrating in phases with stiffer bonds. In general, the stiffest bonds form around atoms with the lowest coordination and the highest valence state. Owing to the bonding environment changes Mo may undergo around ΔIW −1, we have varied oxygen fugacity to investigate whether changes in Mo valence and coordination state affect the fractionation of Mo isotopes.

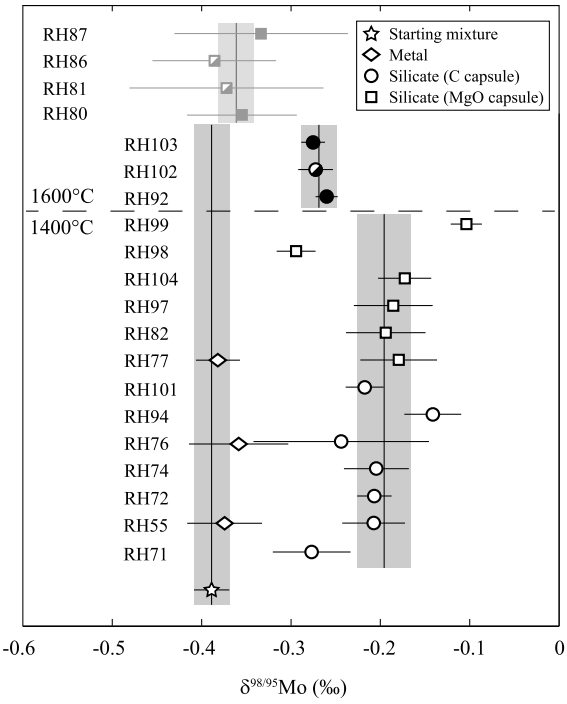

Fig. 3. Molybdenum isotope compositions for starting mixtures and experimental run products. All analysed metals are within uncertainty identical to the bulk composition of starting materials. Open symbols of experimental run products refer to experiments performed at 1400 °C, closed symbols to experiments at 1600 °C. Half-filled symbols represent Sn-free experiments at 1600 °C. Averages (with shades as 95% confidence intervals) are given for 1400 °C and 1600 °C, where two different averages are given for the latter due to disequilibrium fractionation in MgO capsules (grey symbols; see Section 4.2).

The range of oxygen fugacities attainable in our experiments was limited by the amount of Mo in the silicate melt at low oxygen fugacity and by the stability of Fe-based metal at high oxygen fugacity. As experiments in MgO and graphite capsules yielded identical results (see Section 4.1.1), we used both MgO and graphite capsules to vary oxygen fugacity between ΔIW −1.79 and +0.47. Following O'Neill and Eggins (2002), Mo^{4+} should decrease from ∼80% to ∼23% of the total Mo from ΔIW −1.79 to +0.47, respectively, for the silicate melt compositions of our experiments. These percentages are, however, sensitive to uncertainties in Gibbs free energies, mainly for the formation of liquid MoO_2. A 10% increase in the Gibbs free energy of the reaction, for instance, would predict approximately 10% lower Mo^{4+} fractions in our samples (68% and 14% for ΔIW −1.79 to +0.47, respectively).

Despite the variation in oxygen fugacity and the expected corresponding change in valence state, Mo isotope fractionation factors between metal and silicate in our experiments do not vary as a function of oxygen fugacity (Fig. 4b). This could indicate either that Mo isotope fractionation between liquid metal and liquid silicate is insensitive to the bonding environment in the silicate liquid, or that the bonding environment of Mo has not changed significantly in our experiments. The latter can be investigated by regressing oxygen fugacity against elemental Mo distribution. Molybdenum distribution (and isotope fractionation) between metal and silicate occurs by the reaction

$$\mathrm{Mo} + \frac{n}{4}\mathrm{O_2} \rightleftharpoons \mathrm{MoO}_{n/2} \qquad \text{(i)}$$

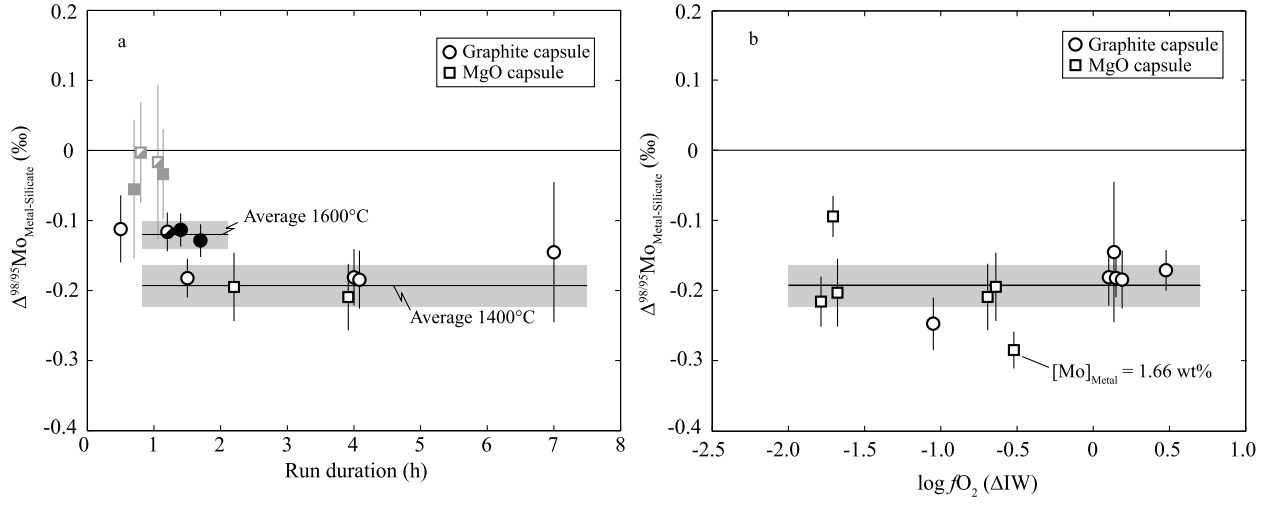

Fig. 4. Molybdenum isotope fractionation factors between metal and silicate plotted against experimental run duration (panel a) and oxygen fugacity (panel b). Errors are 95% confidence intervals. Panel (a) shows that at 1400 °C (open symbols) the shortest run duration of 0.5 h had probably not fully equilibrated. Experiments with longer run duration are within uncertainties identical, independent of whether they were performed in graphite or MgO capsules. Closed symbols in panel (a) represent Sn-bearing experiments at 1600 °C, while half-filled symbols refer to Sn-free experiments at 1600 °C. Experiments at 1600 °C in MgO capsules are in grey, because they represent disequilibrium fractionation (see Section 4.2). Panel (b) shows that Mo isotope fractionation factors are independent of oxygen fugacity in the range from ΔIW −1.79 to +0.47. All experiments presented in panel (b) were performed at 1400 °C. The experiment with 0.5 h run duration was not plotted here, because it probably represents disequilibrium fractionation.

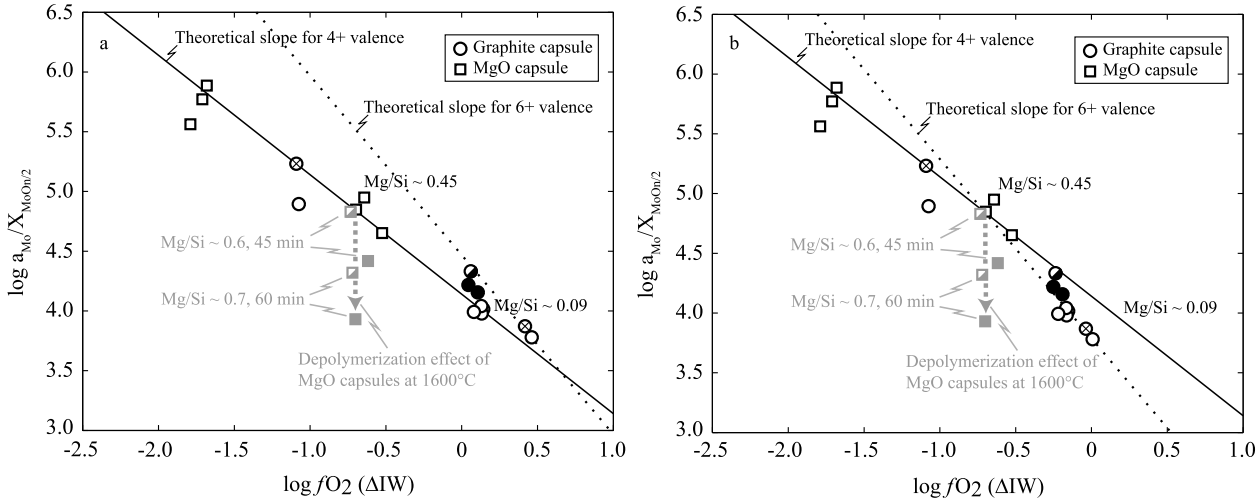

Fig. 5. Determination of Mo valence state as a function of oxygen fugacity. Panel (a) shows elemental partition coefficients as a ratio of Mo metal activity over molar content of Mo-oxide. Oxygen fugacity was calculated with a constant FeO activity coefficient of 1.7 as determined by (Holzheid et al., 1997). Symbols are identical to Figs. 3 and 4, except for the additional circles with crosses inside, which represent experiments that were not analysed for isotopic compositions. Their silicate Mo contents were determined by LA-ICPMS (see electronic Supplementary Material). A regression through the data derived from experiments at 1400 °C gives a slope of $-0.92^{+0.16}_{-0.10}$, which is within uncertainty of the theoretical slope of −1.0 for Mo^{4+} (solid line). The theoretical slope for Mo^{6+} is shown for reference. Panel (b) presents an alternative for panel (a) using variable activity coefficients for FeO after Holzheid et al. (1997) and Richardson (1956): 1.7 for FeO contents <30 wt%, 1.3 for FeO between 30 and 40 wt%, and 1.0 for FeO contents >40 wt%. This approach suggests that Mo^{6+} is present above ΔIW −0.5. Note that in both panels the data for experiments in MgO capsules at 1600 °C (grey symbols) deviate from the correlation displayed by all other data, apparently as a function of run duration and Mg/Si, while experiments in MgO capsules at 1400 °C do not display this behaviour. Analytical uncertainties are always less than twice the symbol sizes.

where n indicates the valence state of Mo. The equilibrium constant (K) for this reaction can be written as

$$K = \frac{[MoO_{n/2}]}{[Mo] f O_2^{n/4}} \quad (4)$$

where f refers to fugacity, while rectangular brackets indicate activities, which are identical to the product of molar fractions (X) and activity coefficients (γ) for each species. The latter can be calculated with solution models, such as those of Ma (2001) for metal activity coefficients. Eq. (4) can be re-written as

$$\log K = -\log \frac{[Mo]}{[MoO_{n/2}]} - \frac{n}{4} \log f O_2 \quad (5)$$

It follows from Eq. (5) that in $\log \frac{[Mo]}{[MoO_{n/2}]}$ versus $\log f O_2$ space, straight lines with slopes of −1.0 or −1.5 correspond to Mo valence states of 4+ or 6+, respectively. A gradual change of valence state should, therefore, result in a curve that changes its slope from −1.0 to −1.5 from low to high oxygen fugacity. Such a gradual change in slope was observed by O'Neill and Eggins (2002).

For our experiments, the logarithms of the ratios of molar Mo activity and molar $MoO_{n/2}$ fraction versus $\log f O_2$ fall on a straight line with a slope of −1.0 if a constant FeO activity coefficient of 1.7 is used for all experiments. This implies a dominant Mo valence state of 4+ in the silicate melt of all experiments (Fig. 5a). This conclusion does not change when molar $MoO_{n/2}$ fractions are converted to molar $MoO_{n/2}$ activities with activity coefficients calculated with the model of Wade et al. (2012), which accounts for variable SiO_2, MgO, Al_2O_3 and CaO contents in the silicate melt. In fact, the variation in Mg/Si ratios of 0.03–0.45 in experiments at 1400 °C has little effect on the Mo distribution: MgO capsules yielded ~35% lower Mo contents in the silicates compared to graphite capsules (Table 3), but none of these data deviate from the trend (Fig. 5a). In contrast to previous work (Farges et al., 2006; Holzheid et al., 1994; O'Neill and Eggins, 2002), however, we do not observe a change in valence in the silicate melt from Mo^{4+} to Mo^{6+} around ΔIW −1. A possible cause for this discrepancy could be the choice for a constant FeO activity coefficient of 1.7. Based on Richardson (1956), it might be more appropriate to decrease the activity coefficient to ~1.3 and ~1.0 for experiments with ~35 and ~49 wt% FeO. Re-plotting the data in Fig. 5a with oxygen fugacities calculated with these lower FeO activity coefficients would allow for some Mo^{6+} (Fig. 5b).

The absence of a correlation of Mo isotope fractionation with oxygen fugacity indicates that all experiments at 1400 °C can be used to calculate an average Mo isotope fractionation factor between metal and silicate. Two samples are outliers compared to all other experiments, although we do not have an explanation for this (Fig. 3). Experiment RH98, for instance, was performed under conditions identical to experiments RH97 and RH104, yet its fractionation factor is smaller: -0.09 ± 0.03‰ compared to -0.20 ± 0.05‰ and -0.22 ± 0.04‰, respectively (Table 3). As the somewhat different results for experiments RH98 and RH99 remain puzzling, we have only excluded experiment RH71 (too short run duration) from the average Mo isotope fractionation factor between metal and silicate at 1400 °C: -0.19 ± 0.03‰ (95% c.i.).

4.2. Fractionation at 1600 °C

In contrast to the results at 1400 °C, there is a resolvable difference at 1600 °C in Mo isotope fractionation between experiments in graphite and MgO capsules. The experiments in graphite capsules yield an average fractionation factor of -0.12 ± 0.02‰ compared to -0.03 ± 0.04‰ in MgO capsules (95% c.i.). This is ultimately the consequence of kinetic fractionation due to diffusion of Mo into a silicate melt whose composition evolved with time in the MgO capsules. The Mo contents of silicate melts from MgO capsules are 2 to 10 times higher compared to those from graphite capsules. These Mo contents are high for the oxygen fugacity at which they were performed and they plot off the slope for Mo^{4+} (Fig. 5). Moreover, the Mo concentrations in silicate melts of the four experiments in MgO capsules increase with run duration and co-vary with increasing Mg/Si ratios (Fig. 5).

The solubility of high valence elements (such as Mo) in silicate melts increases with melt depolymerisation (Ellison and Hess, 1986; Hillgren et al., 1996), by about one order of magnitude from a dacitic to a basaltic melt (Schmidt et al., 2006). The silicate melts in MgO capsules depolymerise with run duration as a consequence

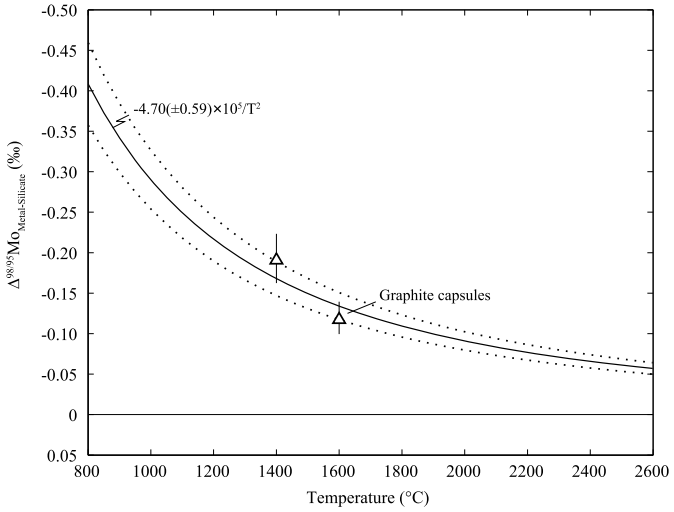

Fig. 6. Temperature dependence of equilibrium Mo isotope fractionation between liquid metal and liquid silicate. The triangles refer to average equilibrium fractionation factors for 1400 °C and 1600 °C with 95% confidence intervals as error bars (see Section 4 for determination of averages). The solid line shows the temperature evolution of the fractionation factor, as derived by weighted $[1/(95\%\ \text{c.i.})^2]$, least-squares regression of Eq. (6) through the average fractionation factors for 1400 and 1600 °C; the stippled lines represent the error envelope (95% c.i.), which reflects the uncertainty (0.59×10^5; determined in the regression) of the empirical constant in $\Delta^{98/95}Mo_{Metal-Silicate} = -4.70(\pm 0.59) \times 10^5/T^2$.

of progressive dissolution of the capsule with time. Consequently, the solubility of Mo also increases progressively during the experiment. This explains the observed dependence of Mo concentrations in silicate melts (run in MgO capsules) on MgO concentration (see Fig. S4 in the electronic Supplementary Material), which increases with temperature and run duration.

The progressively increasing solubility of Mo in the silicate melt leads to progressive oxidation of metallic Mo. If the oxidation rate exceeds the rate of isotopic equilibration, kinetic Mo isotope fractionation is expected to occur. As light isotopes diffuse faster than heavy isotopes, this scenario fits the observation that the silicates from MgO capsules are on average lighter than those recovered from graphite capsules. We therefore conclude that rapid dissolution of capsule-derived MgO led to imperfect equilibration of the silicate melt at 1600 °C in MgO capsules and yielded disequilibrium Mo isotope fractionation. These observations indicate that caution is required when experimentally studying equilibrium isotope fractionation in capsules that are reactive with the studied phases; at least for high valence elements in capsules that are very reactive with a silicate melt.

The equilibrium Mo isotope fractionation factor between liquid metal and liquid silicate at 1600 °C is, therefore, represented by the average fractionation factor determined in graphite capsules: -0.12 ± 0.02‰ (95% c.i.). As expected, this is smaller than the fractionation factor of -0.19 ± 0.03‰ determined at 1400 °C.

5. Implications for studies of core formation

The experiments show that the presence or absence of C or Sn in the metal does not affect Mo isotope fractionation between liquid metal and liquid silicate. Variations in silicate composition also do not seem to affect Mo isotope fractionation, at least in the range from about 40–48 wt% SiO_2, 7.9–49 wt% FeO and 0.85–16 wt% MgO. Additionally, we did not observe an oxygen fugacity dependence of the Mo isotope fractionation factor between ΔIW −1.79 and ΔIW +0.47, of which the lower end is in the range of oxygen fugacities expected for core formation in planetesimals or planetary embryos (Righter and Drake, 1996).

Bigeleisen and Mayer (1947) and Urey (1947) showed that equilibrium, mass dependent fractionation of isotopes decreases as a function of the square of temperature. Based on their work, the Mo isotope fractionation factor between metal and silicate melts can be described as

$$\Delta^{98/95}Mo_{Metal-Silicate} \propto \left(\frac{\Delta m_{98-95}}{m_{98}m_{95}}\frac{\Delta F_{Metal-Silicate}}{T^2}\right)\cdot 1000 \qquad (6)$$

where m_{98} and m_{95} are the atomic masses of ^{98}Mo and ^{95}Mo, respectively, Δm the difference between the isotopic masses, $\Delta F_{Metal-Silicate}$ the difference in force constants of the bonds of the isotopes in the metal and silicate melts, and T the temperature in K. Fitting our average equilibrium fractionation factors for 1400 °C (-0.19 ± 0.03‰) and 1600 °C (-0.12 ± 0.02‰) in Eq. (6), we determine that the Mo isotope fractionation factor between liquid metal and liquid silicate can be described as

$$\Delta^{98/95}Mo_{Metal-Silicate} = \frac{-4.70(\pm 0.59) \times 10^5}{T^2} \qquad (7)$$

As can be seen in Fig. 6, equilibrium Mo isotope fractionation between metal and silicate may be analytically resolvable up to temperatures around 2500 °C, with fractionation decreasing to ~0.05‰ between 2500 °C and 3000 °C. Molybdenum isotopes may therefore constitute a new tool to study the conditions of metal–silicate equilibration and core formation in planetary objects. This approach may be particularly useful for planetesimals and planetary embryos, for which temperatures of core formation are thought to be lower than in large bodies such as the Earth, for which the analytical resolution for determining Mo isotope fractionation (⩽0.06‰ above 2500 °C) might be limiting. As Mo is a refractory element, chondrites represent good analogues for both bulk and core Mo isotope compositions of planetary objects. Temperatures of metal–silicate segregation in planets or on the parent bodies of various achondrites could hence be estimated with the above determined temperature dependence by comparing Mo isotope compositions of chondrites to those of silicate samples of differentiated planetary objects. Preliminary Mo isotope data for chondrites, angrites, and terrestrial and lunar basalts suggest that there may indeed be variations in $\delta^{98/95}$Mo that are related to core formation (Burkhardt et al., 2013). A large advantage of using Mo isotopes to constrain the temperature conditions of core formation, compared to an approach based on siderophile element concentrations, is that Mo isotope fractionation is unambiguously dependent on temperature. Whether Mo isotope fractionation is additionally affected by a slight pressure dependence, which could be relevant for large bodies, remains to be investigated.

6. Conclusions

Our study establishes that:

1. There is equilibrium fractionation of Mo isotopes between liquid metal and liquid silicate. At 1400 °C, the $\delta^{98/95}$Mo value of the silicate melt is 0.19 ± 0.03‰ (95% confidence interval) heavier than that of the metal melt, while it is 0.12 ± 0.02‰ heavier at 1600 °C. The temperature dependence of the Mo isotope fractionation factor ($\Delta^{98/95}$Mo) between liquid metal and liquid silicate can thus be described as $\Delta^{98/95}Mo_{Metal-Silicate} = -4.70(\pm 0.59) \times 10^5/T^2$ (95% c.i.).

2. The addition of C or Sn to the compositional system does not affect Mo isotope fractionation between metal and silicate liquids. Furthermore, Mo isotope fractionation also appears independent of variations in silicate composition for basanitic to basaltic melt compositions. This suggests that mass dependent equilibrium fractionation of Mo isotopes might be largely independent of composition, at least for Fe-based metal and primitive silicate melts.

3. Mo isotope fractionation between metal and silicate liquids is constant over a range of oxygen fugacities from ΔIW −1.79 to +0.47. This is probably because Mo does not substantially change valence state in our experiments over this range of fugacities. It is dominantly present as Mo^{4+}, although Mo^{6+} may be present at our highest oxygen fugacities.

4. Experiments performed at 1600 °C in MgO capsules resulted in silicate melt compositions that were only slightly heavier than metal. Continuous reaction between the MgO capsule and the silicate melt resulted in kinetic enrichment of the silicate in light Mo isotopes, which yielded disequilibrium fractionation due to progressively increasing Mo solubility. This effect of rapid dissolution of MgO from the capsule underlines that caution is required when investigating equilibrium isotope fractionation in capsule material that is reactive with the sample.

5. Mass dependent Mo isotope fractionation constitutes a novel tool to study the conditions of core formation in planetary bodies. The siderophile character of Mo enables direct comparison of Mo isotope compositions of silicate samples to the average of chondrites. The temperatures of core formation implied by Mo isotope fractionation may thus further constrain models of core formation.

Acknowledgements

This study was made possible due to the generous research funding of ETH Zurich. CB was supported by SNF grant No. 2-77213-08. We thank Felix Oberli for the 'Thermo2Nu' program and maintenance of the Nu1700. Mario Fischer-Gödde was of great help for the analyses performed on the Neptune Plus in Münster. Ben Reynolds is greatly thanked for his help with the double spike deconvolution. Bruno Zürcher was indispensable for maintenance on the centrifuging piston cylinder. We appreciate the donation of an aliquot of sample AJ011 by Nicolas Greber. Markus Wälle has provided help with LA-ICPMS analyses. Finally, we thank two anonymous reviewers who helped to improve the manuscript.

Appendix A. Supplementary material

Supplementary material related to this article can be found online at http://dx.doi.org/10.1016/j.epsl.2013.08.003.

References

Bigeleisen, J., Mayer, M.G., 1947. Calculation of equilibrium constants for isotopic exchange reactions. J. Chem. Phys. 15, 261–267.
Burkhardt, C., Hin, R.C., Kleine, T., Bourdon, B., 2013. Mass-dependent molybdenum isotope fractionation—a new tracer for core formation. In: Lunar and Planetary Science Conference. Houston. Abstract #1902.
Burkhardt, C., Kleine, T., Oberli, F., Pack, A., Bourdon, B., Wieler, R., 2011. Molybdenum isotope anomalies in meteorites: Constraints on solar nebula evolution and origin of the Earth. Earth Planet. Sci. Lett. 312, 390–400.
Corgne, A., Keshav, S., Wood, B.J., McDonough, W.F., Fei, Y.W., 2008. Metal–silicate partitioning and constraints on core composition and oxygen fugacity during Earth accretion. Geochim. Cosmochim. Acta 72, 574–589.
Ellison, A.J., Hess, P.C., 1986. Solution behavior of +4 cations in high silica melts—Petrologic and geochemical implications. Contrib. Mineral. Petrol. 94, 343–351.
Farges, F., Siewert, R., Brown, G.E., Guesdon, A., Morin, G., 2006. Structural environments around molybdenum in silicate glasses and melts. I. Influence of composition and oxygen fugacity on the local structure of molybdenum. Can. Min. 44, 731–753.
Fegley, B.J., Palme, H., 1985. Evidence for oxidizing conditions in the solar nebula from Mo and W depletions in refractory inclusions in carbonaceous chondrites. Earth Planet. Sci. Lett. 72, 311–326.
Georg, R.B., Halliday, A.N., Schauble, E.A., Reynolds, B.C., 2007. Silicon in the Earth's core. Nature 447, 1102–1106.
Greber, N.D., Hofmann, B.A., Voegelin, A.R., Villa, I.M., Nagler, T.F., 2011. Mo isotope composition in Mo-rich high- and low-T hydrothermal systems from the Swiss Alps. Geochim. Cosmochim. Acta 75, 6600–6609.
Greber, N.D., Siebert, C., Nägler, T.F., Pettke, T., 2012. $\delta^{98/95}$Mo values and molybdenum concentration data for NIST SRM 610, 612 and 3134: Towards a common protocol for reporting Mo data. Geostand. Geoanal. Res. 36 (3), 291–300.
Hillgren, V.J., Drake, M.J., Rubie, D.C., 1996. High pressure and high temperature metal–silicate partitioning of siderophile elements: The importance of silicate liquid composition. Geochim. Cosmochim. Acta 60, 2257–2263.
Hin, R.C., Schmidt, M.W., Bourdon, B., 2012. Experimental evidence for the absence of iron isotope fractionation between metal and silicate liquids at 1 GPa and 1250–1300 °C and its cosmochemical consequences. Geochim. Cosmochim. Acta 93, 164–181.
Holzheid, A., Borisov, A., Palme, H., 1994. The effect of oxygen fugacity and temperature on solubilities of nickel, cobalt, and molybdenum in silicate melts. Geochim. Cosmochim. Acta 58, 1975–1981.
Holzheid, A., Palme, H., Chakraborty, S., 1997. The activities of NiO, CoO and FeO in silicate melts. Chem. Geol. 139, 21–38.
Jana, D., Walker, D., 1997. The impact of carbon on element distribution during core formation. Geochim. Cosmochim. Acta 61, 2759–2763.
Karato, S., Murthy, V.R., 1997. Core formation and chemical equilibrium in the Earth—I. Physical considerations. Phys. Earth Planet. Inter. 100, 61–79.
LaTourrette, T., Wasserburg, G.J., Fahey, A.J., 1996. Self diffusion of Mg, Ca, Ba, Nd, Yb, Ti, Zr, and U in haplobasaltic melt. Geochim. Cosmochim. Acta 60, 1329–1340.
Lazar, C., Young, E.D., Manning, C.E., 2012. Experimental determination of equilibrium nickel isotope fractionation between metal and silicate from 500 to 950 °C. Geochim. Cosmochim. Acta 86, 276–295.
Li, J., Agee, C.B., 1996. Geochemistry of mantle–core differentiation at high pressure. Nature 381, 686–689.
Ma, Z.T., 2001. Thermodynamic description for concentrated metallic solutions using interaction parameters. Metall. Mater. Trans. B 32, 87–103.
Mizuike, A., 1983. Enrichment Techniques for Inorganic Trace Analysis. Springer, Berlin.
Moynier, F., Yin, Q.Z., Schauble, E., 2011. Isotopic evidence of Cr partitioning into Earth's core. Science 331, 1417–1420.
O'Neill, H.S.C., Eggins, S.M., 2002. The effect of melt composition on trace element partitioning: an experimental investigation of the activity coefficients of FeO, NiO, CoO, MoO_2 and MoO_3 in silicate melts. Chem. Geol. 186, 151–181.
Okamoto, H., 1993. Phase Diagrams of Binary Iron Alloys. ASM International, Materials Park, Ohio.
Poitrasson, F., Roskosz, M., Corgne, A., 2009. No iron isotope fractionation between molten alloys and silicate melt to 2000 °C and 7.7 GPa: Experimental evidence and implications for planetary differentiation and accretion. Earth Planet. Sci. Lett. 278, 376–385.
Richardson, F.D., 1956. Activities in ternary silicate melts. Trans. Faraday Soc. 52, 1312–1324.
Righter, K., Drake, M.J., 1996. Core formation in Earth's Moon, Mars, and Vesta. Icarus 124, 513–529.
Righter, K., Pando, K.M., Danielson, L., Lee, C.T., 2010. Partitioning of Mo, P and other siderophile elements (Cu, Ga, Sn, Ni, Co, Cr, Mn, V, and W) between metal and silicate melt as a function of temperature and silicate melt composition. Earth Planet. Sci. Lett. 291, 1–9.
Rubie, D.C., Frost, D.J., Mann, U., Asahara, Y., Nimmo, F., Tsuno, K., Kegler, P., Holzheid, A., Palme, H., 2011. Heterogeneous accretion, composition and core–mantle differentiation of the Earth. Earth Planet. Sci. Lett. 301, 31–42.
Rudge, J.F., Kleine, T., Bourdon, B., 2010. Broad bounds on Earth's accretion and core formation constrained by geochemical models. Nat. Geosci. 3, 439–443.
Schauble, E.A., 2004. Applying stable isotope fractionation theory to new systems. Rev. Mineral. Geochem. 55, 65–111.
Schmidt, M.W., Connolly, J.A.D., Gunther, D., Bogaerts, M., 2006. Element partitioning: The role of melt structure and composition. Science 312, 1646–1650.
Schoenberg, R., Zink, S., Staubwasser, M., Von Blanckenburg, F., 2008. The stable Cr isotope inventory of solid Earth reservoirs determined by double spike MC-ICP-MS. Chem. Geol. 249, 294–306.
Shahar, A., Hillgren, V.J., Young, E.D., Fei, Y.W., Macris, C.A., Deng, L.W., 2011. High-temperature Si isotope fractionation between iron metal and silicate. Geochim. Cosmochim. Acta 75, 7688–7697.
Siebert, C., Nagler, T.F., Kramers, J.D., 2001. Determination of molybdenum isotope fractionation by double-spike multicollector inductively coupled plasma mass spectrometry. Geochem. Geophys. Geosyst. 2. Art. no. 2000GC000124.
The Japan Society for the Promotion of Science, the 19th Committee on Steelmaking, 1988. Steelmaking Data Sourcebook, Part 2: Recommended Values of Activity and Activity Coefficients, and Interaction Parameters of Elements in Iron Alloys. Gordon and Breach Science Publishers, Montreux.
Taylor, G.J., Keil, K., Mccoy, T., Haack, H., Scott, E.R.D., 1993. Asteroid differentiation—Pyroclastic volcanism to magma oceans. Meteoritics 28, 34–52.
Urey, H.C., 1947. The thermodynamic properties of isotopic substances. J. Chem. Soc., 562–581.
Wade, J., Wood, B.J., Tuff, J., 2012. Metal–silicate partitioning of Mo and W at high pressures and temperatures: Evidence for late accretion of sulphur to the Earth. Geochim. Cosmochim. Acta 85, 58–74.
Wood, B.J., Walter, M.J., Wade, J., 2006. Accretion of the Earth and segregation of its core. Nature 441, 825–833.
Zhu, X.K., Guo, Y., Williams, R.J.P., O'Nions, R.K., Matthews, A., Belshaw, N.S., Canters, G.W., de Waal, E.C., Weser, U., Burgess, B.K., Salvato, B., 2002. Mass fractionation processes of transition metal isotopes. Earth Planet. Sci. Lett. 200, 47–62.